Results in Physics 75 (2025) 108341

Contents lists available at ScienceDirect

Results in Physics

journal homepage: www.elsevier.com/locate/rinp

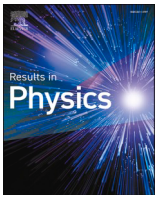

The (temperature-dependent) Raman spectra of some traditional semiconductors

A.R. Zanatta

Instituto de Física de São Carlos, USP, São Carlos 13560-970 SP, Brazil

ARTICLE INFO

Keywords:
Raman spectroscopy
Temperature-dependence
Semiconductor materials

ABSTRACT

Semiconductor materials represent the core of many modern technological applications and they are expected to continue influencing the ever-growing field of data generation-transmission-processing. This can be reached by means of new materials and/or devices but, especially, by precisely recognizing (and controlling) some of their main properties. In this regard, Raman scattering spectroscopy can contribute with important structural-electronic information by probing the phonon behavior – even in well-known semiconductors – over a wide temperature range. Accordingly, this work presents a comprehensive investigation of the Raman spectra of 15 semiconductors (Si, Ge, SiC, GaN, GaP, GaAs, GaSb, InP, InAs, ZnO, ZnS, ZnSe, ZnTe, CdS, and TiO_2) comprising IV-IV, III-V and II-VI compounds and different crystal structures (diamond, zinc blende, wurtzite, and rutile). Based on these spectra, all phonon modes were identified and the most prominent ones were analyzed in terms of their peak position (ω) and line-width (γ), in the 83–823 K temperature range, as obtained from fitting the spectra with Voigt functions. This part of the work includes a detailed study of the temperature-dependent $\omega(T)$ and $\gamma(T)$ data according to the 3- and 4-phonon model, as well as their (supposedly) linear behavior above room-temperature. In the former case it was possible (at least qualitatively) to separate the contributions due to the anharmonic phonon–phonon interactions from the thermal expansion effects. In the latter, the results suggest an apparent relationship between the linear $d\omega/dT$ and $d\gamma/dT$ slopes and the optical bandgaps E_{gap}'s (and their corresponding linear dE_{gap}/dT slopes) of the various semiconductor samples – regardless of the compound type or crystal structure. The most likely origins of these relationships are discussed, and their potential in proposing the most suitable materials and/or operation conditions for device applications (as temperature probes or tunable optical filters, for instance) are briefly outlined.

Introduction

Following the historical tool-making (Stone, Bronze and Iron) Ages and social-cultural (Classical, Medieval, Early Modern and Modern) Eras, maybe, future generations will acknowledge the period starting in the ~1900′s as the Semiconductor (or Silicon) Age. In fact, even though contemporary civilization relies on a huge variety of materials including new alloys, ceramics, plastics, C-based, low-dimensional structures, etc., it seems very unlikely to conceive modern life without the presence of (micro-)electronics devices, in which the semiconductor materials (and silicon, in particular) are essential [1–3]. It happens because of the semiconductors unique properties (as derived from their atom bonding and corresponding electronic states [4,5]) that allow the manipulation of electrons in order to, accurately, generate-transmit-process the so-called digital information. Furthermore, electrons in elemental semiconductor (and devices) are known to be susceptible to external temperature and radiation circumstances, for example, in which cases phonons play a considerable role [6–10].

Phonons, or lattice vibrations, are related to practically all the thermal properties of a solid and are the reason of either desirable (photon absorption in indirect optical processes) or unwanted (charge scattering in electrical transport) outcomes in semiconductor materials [11]. Moreover, the main characteristics of phonons (and, ultimately, of the semiconductor materials) can be investigated in great detail by probing their behavior under various different (temperature, pressure, polarization, etc.) conditions by means of standard spectroscopic techniques such as infrared absorption and Raman scattering, for example [12–14]. Raman spectroscopy, in particular, is based on the process of inelastic light scattering experienced by incoming (monochromatic) photons as a result of their interaction with the vibrations (phonons) of bonded atoms. This photon-phonon interaction depends on the bond polarizability, or ease of distorting the bonding electrons from their

E-mail address: zanatta@ifsc.usp.br.

https://doi.org/10.1016/j.rinp.2025.108341
Received 20 March 2025; Received in revised form 6 June 2025; Accepted 21 June 2025
Available online 22 June 2025

original positions, of the lattice that is being probed [15], and it gives rise to scattered photons presenting slightly lower (Stokes shift) and higher (anti-Stokes shift) energy variations. Since the bond polarizability is related to the chemical aspects of the matter (*i.e.*, electron density, bond strength and length), these characteristics will be noticeable in the Raman scattered signals [16]. For practical reasons, it is usual to consider the Raman Stokes signals whose analysis, comprising their relative intensities and spectral frequencies and line-shapes, can reveal details of the matter (solid, liquid, gas, (in)organic, etc.) under investigation. This is the case of semiconductors, in which the analysis of the Raman spectra gives the main characteristics of the existing phonons as well as, in a temperature-dependent experiment, the phonon dynamics. In combination with some other property (like the optical bandgap, for instance), the information provided by Raman spectroscopy can be used to indicate the ideal semiconductor type and conditions in order to obtain the best results in a specific device application. This kind of associative study represents the main focus of the present work in which the Raman and optical results of several semiconductors are grouped together to find some interesting trend that can be useful in the development of new-improved optoelectronic devices.

For the sake of comprehensiveness, the following paragraphs introduce some basic properties and the most common uses of the semiconductors considered in this work that, certainly, will be useful to those engaged in the experimental research and development (R&D) on these materials. Very detailed information can be achieved from standard text-books [4–11], as well as from a series of classical handbooks relating IV-IV and III-V compounds [17,18], II-VI compounds [18–20], and TiO_2 [18,21]. In addition to these, the optical bandgap E_{gap} values and properties of all semiconductors can be found in [22,23].

(Column) IV-IV-based materials

Silicon (Si) – Presenting a diamond structure and an indirect optical bandgap E_{gap} = 1.10 eV, Si is known by its singular (though modest) properties that, allied to its natural abundance, justify its widespread use in (micro-) electronics [3] and in photovoltaic PV solar cells [24,25]. More recently, the applications involving Si have been expanded to the generation, routing, modulation, processing and detection of light, or Si-photonics [26], as well as to Si-quantum-computing [27,28].

Germanium (Ge) – Also of diamond structure and exhibiting indirect (0.67 eV) and direct (0.80 eV) E_{gap}'s, Ge was broadly applied in Schottky diodes during the World War II and it was responsible for the very first transistor [2]. Ge has also found applications in (micro-)electronics, (special) radiation detectors and PV solar cells [29]. Similar to Si, in the effort to develop disruptive quantum technologies, Ge is emerging as a versatile material to realize devices capable of encoding, processing and transmitting quantum information [30].

Silicon carbide (SiC) – SiC is a IV–IV compound semiconductor with E_{gap} in the 2.3–3.3 eV range (depending on the crystal structure, or polytype) that can operate at considerably high voltage, switching frequency and temperature. Among other wide E_{gap} semiconductors, SiC is exceptional because it can be easily doped (either p- or n-type) and its native oxide is SiO_2 – the same insulator as in Si [31]. This makes it possible to fabricate, for example, the entire family of MOS-based (metal–oxide–semiconductor) electronic devices in SiC [32].

Diamond (diam) – (Even though diamond has not been measured in this work, occasionally, their results will be considered for comparison reasons.) As the name suggests, it presents the diamond structure (as the result of C sp^3 bonds), E_{gap} = 5.47 eV, and extraordinary chemical-physical-thermal properties [33]. So far, a wide variety of manufacturing methods have been developed to deposit diamond layers and structures – the most common is the chemical vapor deposition (CVD) [34] – rendering applications that can vary from protective (hard) coatings to (high power) electronic devices [35].

III-V-based materials

Gallium nitride (GaN) – Owing to its crystal structure (wurtzite) and wide direct bandgap (E_{gap} = 3.40 eV), GaN has long been considered for its potential use in high power electronics and in optoelectronic devices [36]. Allied to its relative simple production methods and success in providing commercial blue light emitting devices, there is a lot of R&D on GaN (and on its heterostructures with other nitride semiconductors) [37].

Gallium phosphide (GaP) – Part of the interest in GaP (and its alloys) arises from its zinc blende lattice (that perfectly matches with Si) and indirect optical E_{gap} in the visible range (2.25 eV), aiming at the development of light emitting sources [38] and, more recently, on biomedical and on quantum technologies [39].

Gallium arsenide (GaAs) – Perhaps the most known manmade III-V semiconductor, GaAs is characterized by its zinc blende structure, a direct E_{gap} = 1.43 eV, and great adaptability in providing heterostructures exhibiting high electron mobility and superior optical (light emission) properties [40]. As a result, GaAs has been considered in applications like transistors (under the most varied geometries-concepts), Gunn and laser diodes, and high-efficiency solar cells, just to mention a few of them [41].

Gallium antimonide (GaSb) – Historically, the R&D of various III–V semiconductors were dedicated to optoelectronics and, in most of the cases, they were closely related with the wavelength of the optical fiber loss minima [42]. That is the case of GaSb (a compound with zinc blende structure and direct E_{gap} around 0.70 eV [43]), that can be employed in conjunction with many semiconductors such as (AlGa)Sb or In(AsSb) and that has potential for detectors, lasers and quantum well structures operating in the (near-)infrared spectral region [44].

Indium phosphide (InP) – Like all III-V compound semiconductors, InP (zinc blende structure and E_{gap} = 1.32 eV) has found numerous applications in the field of optics and electronics – including those devoted to solar energy conversion [45]. In the last few years, the interest has also been focused in producing efficient (non-toxic, tunable optical bandgap) quantum dots [46] and quantum dot light emitting diodes QLED's [47], for example.

Indium arsenide (InAs) – Also presenting a zinc blende structure and a bandgap in the infrared spectral range (E_{gap} = 0.36 eV) [48], InAs-based quantum dots QD's are promising building blocks for numerous photonic (in the infrared spectral range) and biomedical (RoHS-compliant) applications [49].

II-VI-based materials

The combination of Zn or Cd (group II elements) with O, S, Se, or Te (group VI elements) originates the so-called II-VI semiconductor materials. They are known to present E_{gap}'s in the 2−4 eV range and, because of their ease of production, II-VI-based materials have been systematically investigated aiming applications in photonics, catalysis and biomedical science. Moreover, since the crystal shape and size of these materials directly influence their physical–chemical properties and interaction with biological systems, most of the efforts in the field rely on the R&D of micro/nano-structured materials, namely: in the form of thin films, nano-crystals, or QD's, for example.

Zinc oxide (ZnO) – The first scientific reports on ZnO date from the 1930's (revealing its wurtzite structure and lattice parameters) and they evolved to the determination of its optical (E_{gap} = 3.20 eV) and vibrational properties, as well as to its synthesis and production of simple electronic devices [50]. At present, ZnO-based materials can be obtained from various different methods (metal–organic chemical vapor deposition, (reactive) sputtering, molecular beam epitaxy, pulsed laser deposition, atomic layer epitaxy, etc.) and most of their applications involve the development of light emitting sources operating in the ultra-violet−blue spectral range [51].

Zinc sulfide (ZnS) – ZnS is a naturally occurring salt that can exist

under the zinc blende (spharelite) and wurtzite forms. It is the main source of zinc and most commonly used as a pigment for paints, plastics, and rubber [52]. Because of its optical properties (direct $E_{gap} = 3.60$ eV) it has been largely considered for luminescent-scintillation purposes and, in recent years, in the development of electroluminescent devices and semiconductor QD's [53].

Zinc selenide (ZnSe) – Along with ZnS, ZnSe is among the first discovered semiconductors that, owing to its zinc blende structure and direct $E_{gap} = 2.65$ eV, represents an important material for the fabrication of devices like PV solar cells, and LED's and lasers operating in the blue–green spectral range [52], as well as in luminescent core–shell structures [54].

Zinc teluride (ZnTe) – Like ZnS and ZnSe, ZnTe presents a zinc blende structure, wide direct bandgap ($E_{gap} = 2.25$ eV) and, therefore, various applications in the semiconductors industry (PV solar cells, LED's and lasers, and microwave generators) [52]. The structural-electronic properties of ZnTe has also been explored in order to produce special photodetectors [55].

Cadmium sulfide (CdS) – CdS exhibits a wurtzite structure and a direct optical bandgap in the visible ($E_{gap} = 2.25$ eV) spectral range that, allied to its excellent thermal and chemical stability, justifies its broad use in PV solar cells and (LED's and laser) light sources, for example [52]. Taking advantage of its production methods (in the search for new optical-electronic properties), nanostructures of CdS-based materials has also received considerable attention [56].

Titanium dioxide (TiO_2) – TiO_2 does not fit any of the previous classes of materials. It is a binary transition-metal oxide usually found in three main crystalline polymorphs: Anatase, Rutile and (the less common) Brookite. Each of them presents specific structural-electronic properties and, therefore, semiconducting properties that eventually will be adequate for different (environmentally friendly) applications. In the present work, only the Rutile crystal structure (TiO_2-R) has been considered in detail. In part, this is because of its direct E_{gap} in the visible ($\sim$ 3 eV) spectral range that is suitable for applications in the fields of solar energy conversion [57] and photo-catalysis [58].

After this short phonon – semiconductor overview, the following sections will show the information regarding the Raman measurements, the samples details, and the experimental results they provided. Then, the temperature-dependent Raman results will be discussed in view of some basic properties of the semiconductor materials (like typical bond energy and optical bandgap). Finally, the importance of the present findings in selecting the most convenient semiconductor – application combination will be pointed out.

Experimental

The samples investigated in this work correspond to 15 semiconductors presenting different crystal structures: diamond (Ge and Si), zinc blende (GaAs, GaP, GaSb, InAs, InP, ZnS, ZnSe, and ZnTe), wurtzite (CdS, GaN, 4H-SiC, and ZnO), and rutile (TiO_2). In most of the cases the samples correspond to undoped, 2 sides (mirror) polished, single crystals with thicknesses in the 0.3–1 mm range. The samples were purchased from a semiconductor crystals-wafers supplier and their main characteristics (crystal details and orientation, as well as some physical and electrical properties) can be found in SuppInfo_SamplesDetails.

The Raman measurements were carried out in a commercial setup (*Renishaw* RM2000) by exciting the samples with 632.8 nm photons (backscattering geometry and no preferential polarization). The spectra were acquired in the 83–823 K temperature range (in steps of either 25 or 50 K) by means of a computer-controlled temperature-stage (*Linkam* THMS600). In this case, a 50x long-working distance objective lens (NA = 0.55) and a laser power density of $\sim$ 0.4 mW μm^{-2} have been applied. The study considered the spectra taken from different regions of the samples, as well as a dwell time of 3 min (at the desired temperature) to guarantee thermal equilibrium conditions.

After identification of the main phonon modes, their peak position (or frequency) ω and line-width (or full width at half maximum FWHM height value) γ were determined by fitting the spectra with a combination of Lorentzian and Gaussian profiles. The resulting line-shape is a Voigt function, according to which the true (Lorentzian) phonon line-width can be separated from the (Gaussian) experimental spectrometer resolution [59,60]. Given that the Raman spectra were taken with 632.8 nm photons and a 1200 l mm^{-1} diffraction grating, the spectral resolution (or FWHM in the Gaussian profile) corresponds to 1.6 cm^{-1} [61]. Besides, whenever appropriate, the fitting procedure was preceded by removing some background – always by means of a straight line beneath the experimental spectrum – and by considering the (occasional) presence of nearby phonon contributions. Accordingly, henceforth, the ω (or peak position) and γ (or peak line-width) values correspond to the center of the Voigt function and to the sum of the FWHM of the Lorentzian and Gaussian profiles, respectively.

Results

Fig. 1 shows the room-temperature (RT) Raman spectra of the samples investigated in this work. The spectra were (arbitrarily) distributed into three panels in order to highlight the main phonon contributions (in the 50–1000 cm^{-1} range) of the various semiconductors.

The most intense Raman peaks in Fig. 1 correspond to the following phonon modes – in which the conventional transverse (T), longitudinal (L), optical (O) and acoustic (A) phonon notation applies: **GaSb** ω_{LA} (at $\sim$ 151.6 cm^{-1}) [62], **GaAs** ω_{LO} (at $\sim$ 292.3 cm^{-1}) [63], **GaP** ω_{LO} (at $\sim$ 403.3 cm^{-1}) [63], **GaN** ω_{TO} under E_2 –*high* symmetry (at $\sim$ 568.7 cm^{-1}) [64], rutile **TiO_2** ω_{LO} under A_{1g} symmetry (at $\sim$ 611 cm^{-1}) [65,66], **ZnTe** ω_{TO} (at $\sim$ 177.8 cm^{-1}) [67,68], **ZnSe** ω_{LO} (at $\sim$ 253.5 cm^{-1}) [67–69], **ZnS** ω_{LO} (at $\sim$ 351.5 cm^{-1}) [70], **ZnO** E_2 –*high* (at $\sim$ 439.3 cm^{-1}) [71–73], **Si** ω_{TO} (at $\sim$ 521.5 cm^{-1}) [74], **InAs** ω_{LO} (at $\sim$ 236.4 cm^{-1}) [75], **CdS** ω_{LO} (at $\sim$ 301.5 cm^{-1}) [76], **Ge** ω_{TO} (at $\sim$ 302.7 cm^{-1}) [77], **InP** ω_{LO} (at $\sim$ 347.2 cm^{-1}) [63], and **4H-SiC** ω_{TO} under $E_2(TO)$ symmetry (at $\sim$ 777.4 cm^{-1}) [78]. The above assignments were based on the literature and took into account the excitation wavelength (632.8 nm), the backscattering geometry, the use of no preferential polarization and the crystal orientation of the samples (see SuppInfo_SamplesDetails). The identification of all phonon modes exhibited by the considered semiconductors (and their corresponding references) is given in SuppInfo_FormalAnalysis.

Owing to the phonon susceptibility to anharmonic interactions and/or resulting from thermal expansion effects, the study of the temperature-dependent ω and γ data can provide important structural information [79]. Usually, the analysis of $\omega(T)$ and $\gamma(T)$ is based on the decay of one phonon into two (3-phonon process) and three phonons (4-phonon process), as determined by the Bose-Einstein phonon population [59,80]. This was the approach considered in the present work whose results, along with the experimental $\omega(T)$ and $\gamma(T)$ data – as obtained from fitting the Raman spectra with Voigt functions, in the 83–823 K temperature range – are shown, for example, for the Si semiconductor sample in Fig. 2.

As can be seen, the theoretical model is able to reproduce the experimental $\omega(T)$ and $\gamma(T)$ data with great precision and it allows to differentiate the anharmonic (ω_{PC}) from the lattice expansion (ω_{TE}) contributions (Fig. 2(b)). Further details concerning the 3- and 4-phonon model and the analysis of the $\omega(T)$ and $\gamma(T)$ of the whole series of samples are available in SuppInfo_FormalAnalysis. There, the reader can see all the quantities related to the model, as well as the $\omega(T)$ and $\gamma(T)$ theoretical behavior expressed in terms of $\Delta\omega(T) = \omega(T) - \omega_0$ (Fig. S16) and $\Delta\gamma(T) = \gamma(T) - \gamma_0$ (Fig. S17) – where ω_0 and γ_0 stand for the Raman peak position and line-width at T $\sim$ 0 K. The information supplied by the 3- and 4-phonon model are very illustrative in describing the Raman (T) data but, in certain cases, they could be influenced by: the quality of the experimental data (specially at low temperatures), the absence of (reliable) Grüneisen parameters and/or linear thermal expansion coefficients, as well as by the data fitting procedure [81]. Being aware of

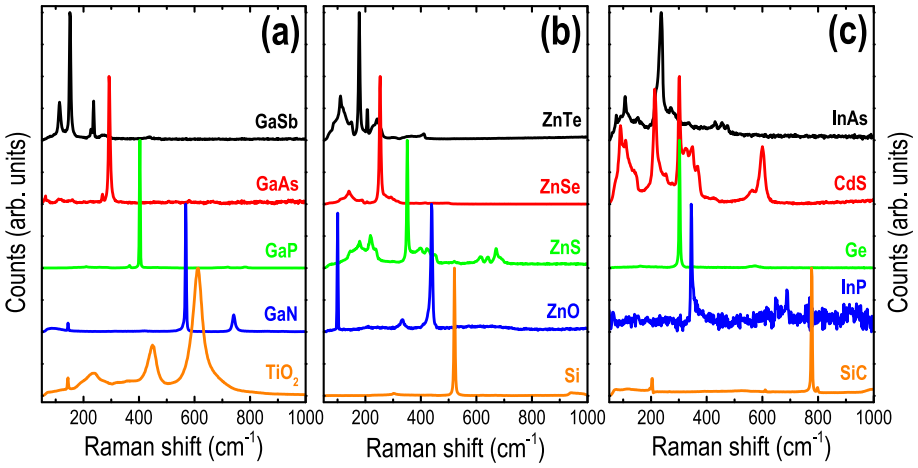

Fig. 1. Raman scattering spectra (in the 50−1000 cm^{-1} range) of all semiconductors considered in this work. The spectra were taken at room-temperature and, for clarity reasons, they were normalized, vertically shifted and separated into three panels.

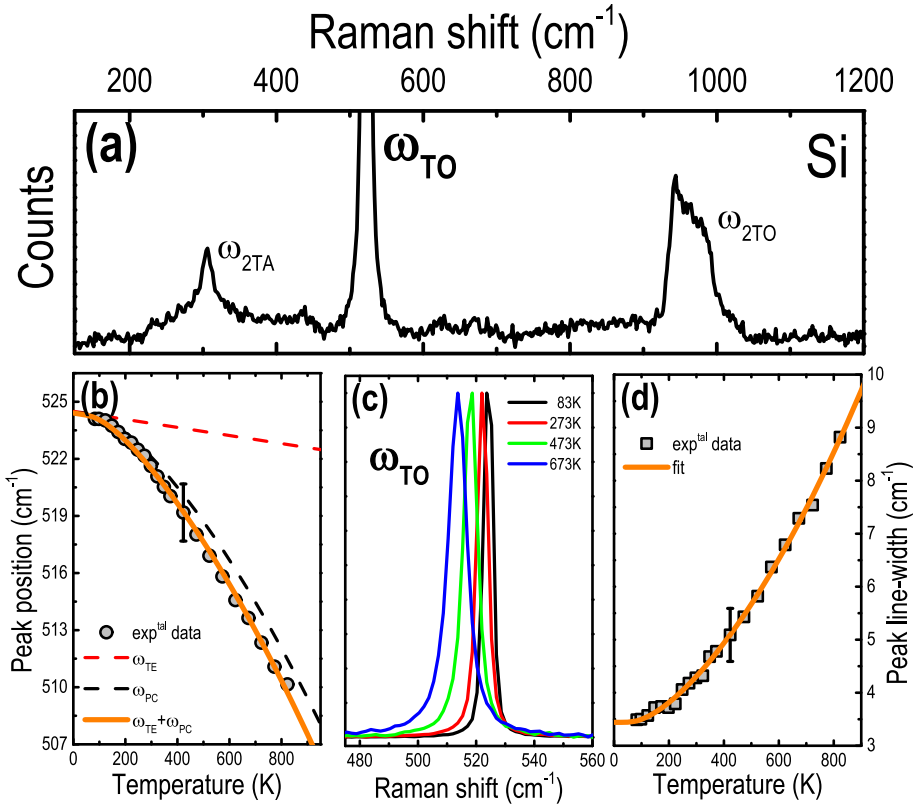

Fig. 2. (a) Room-temperature Raman spectrum of a Si(100) semiconductor sample, indicating its main phonon modes: ω_{2TA} (at ~ 304.5 cm^{-1}), ω_{TO} (at ~ 521.5 cm^{-1}), and ω_{2TO} (at ~ 963.4 cm^{-1}). (b) Experimental peak position $\omega(T)$ in the 83−823 K range, along with its theoretical thermal expansion (ω_{TE}) and phonon coupling (ω_{PC}) contributions. (c) Raman spectra of Si(100), highlighting the ω_{TO} mode, at 83, 273, 473 and 673 K. (d) Experimental peak line-width $\gamma(T)$ in the 83−823 K range, together with its corresponding theoretical curve (fit). The error bars in (b) and (d) comprise typical experimental uncertainty and data fitting dispersion.

these aspects, henceforth, we decided to discuss only the above room-temperature $\omega(T)$ and $\gamma(T)$ experimental data that, conveniently, have been supposed to present a linear behavior. The results of this linear least squares fitting of $\omega(T)$ and $\gamma(T)$ are shown in Figs. 3 and 4 that, for comparison reasons, display $\Delta\omega(T) = \omega(T) - \omega(RT)$ and $\Delta\gamma(T) = \gamma(T) - \gamma(RT)$.

The room-temperature peak position $\omega(RT)$ and line-width $\gamma(RT)$ values, and above RT $d\omega/dT$ and $d\gamma/dT$ linear slopes of all samples can be seen in detail in SuppInfo_LinearFit.

According to Fig. 3, it is clear the decrease of the Raman peak position ω as the temperature advances. It occurs mainly because of the phonon–phonon interaction processes (and to a lesser extent due to lattice expansion effects) and it is common to all samples − see Figs. S1-to-S15 in SuppInfo_FormalAnalysis.

The effect of increasing temperatures, and consequent augment of the phonon–phonon interactions, is also behind the systematic augment observed in the γ Raman line-widths (Fig. 4). At this point it is curious to notice the apparent lack of connection between the $\Delta\omega(T)$ and $\Delta\gamma(T)$

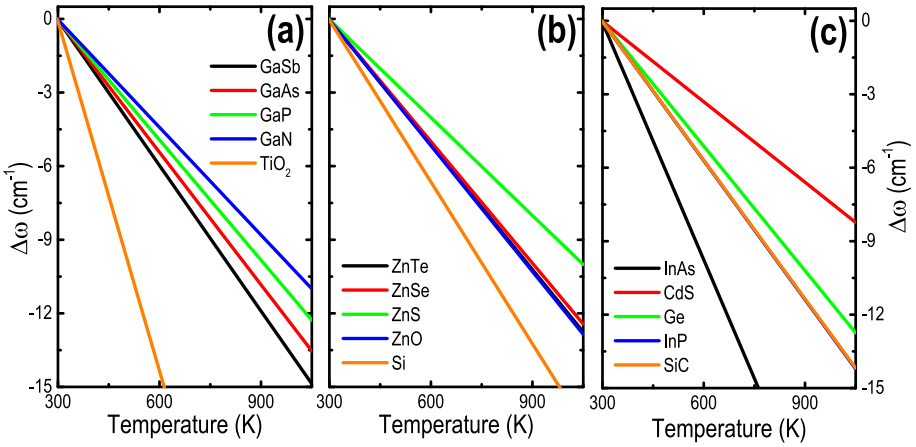

Fig. 3. Linear, above RT, temperature-dependent variation experienced by the Raman peak position ω of the samples investigated in this work. The curves (300−1050 K range), as obtained from the linear least squares fit of the $\omega(T)$ experimental data, correspond to $\Delta\omega(T) = \omega(T) - \omega(RT)$.

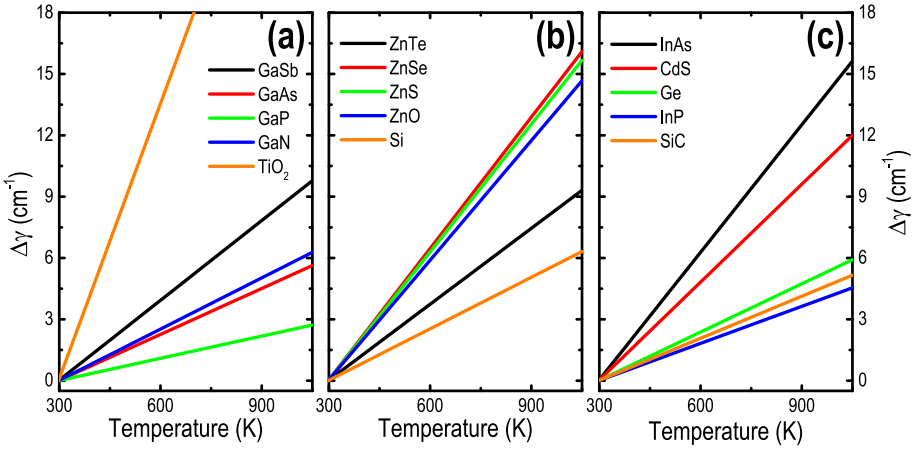

Fig. 4. Linear, above RT, temperature-dependent variation experienced by the Raman peak line-width γ of the samples investigated in this work. The curves (300−1050 K range), as obtained from the linear least squares fit of the $\gamma(T)$ experimental data, correspond to $\Delta\gamma(T) = \gamma(T) - \gamma(RT)$.

behavior presented by the various samples. More specifically: whereas TiO_2 and InAs present the highest $\Delta\omega(T)$ (Fig. 3(a) and (c)) and $\Delta\gamma(T)$ variations (Fig. 4(a) and (c)), that is not the case with Si in which the highest $\Delta\omega(T)$ and lowest $\Delta\gamma(T)$ changes apply (Figs. 3(b) and 4(b)). It happens as a result of differences in the chemical-physical characteristics of each semiconductor and they will be considered in the next section.

Discussion

Roughly speaking, a Raman spectrum shows the magnitude and typical frequency of photons that have been scattered after a beam of monochromatic radiation interacts with matter. It contains features of both elastically (Rayleigh) and inelastically (Stokes and anti-Stokes) photons and it is dependent on the chemical-physical details of the matter. In most of the cases (which involve the particulars of the experimental setup and desired information [14]), it is usual to consider just the Raman Stokes scattered photons, or those ones presenting a frequency (or energy) slightly lower than that of the incoming monochromatic radiation. Within this context, a typical Raman spectrum presents the amount of scattered photons as a function of their frequency shift – as referred to the incoming light excitation. From the microscopic point of view, the incoming photons interact with the matter and distort (polarize) the cloud of electrons around the nuclei to form a short-lived (virtual) state, that is not stable so the photon is quickly re-radiated (scattered) [8,12,14,16,82]. If only electron cloud distortion occurs the photons will be scattered almost unchanged (Rayleigh). However, if nuclear motion is induced, energy will be transferred either from the incident photon to the matter (Stokes), or from the matter to the scattered photon (anti-Stokes). Whether the matter is in a gaseous, liquid, or solid phase it affects the overall strength and band shape of the scattered signal in the Raman spectrum and, in general, solid media give rise to sharp, strong Raman spectra whilst liquids and vapors tend to present weaker (and, sometimes, broader) spectra. Still from the microscopic point of view, the frequencies (or energies) of the scattered photons are dictated by the quantum or vibronic levels representing the matter – specially those associated with the chemical bonds in molecules and solids. An extremely simple (but very descriptive) way to conceive this process is by considering the chemical bond, ideally, as two masses connected by a spring in the form of a quantum harmonic oscillator. According to this approach, in the case of a diatomic molecule, the frequencies of the scattered photons ω (as usually given in terms of the inverse of wavenumbers, or cm^{-1}) can be predicted by $\omega = \frac{1}{c}\sqrt{\frac{K}{\mu}}$, where: c stands for the velocity of light, K is the force constant (or bond strength) and μ is the reduced mass of the atoms involved. When the approach is applied to a solid (or to a collection of bonded-interacting molecules), for example, the incoming radiation induces vibrations through the whole atom lattice. As a result, the scattered photons can present frequencies resulting from vibrations induced along the direction of propagation of the incoming radiation (longitudinal or L modes)

and/or at right angles to it (transverse or T modes). These modes form all through the whole atom lattice and each one consists of a very large number of vibrations of similar energy which occupy a band of energies in the matter. Moreover, depending on the specifics of the radiation–matter interaction, these modes can present frequencies either in the low (acoustic A) or high (optical O) ranges of energy and, therefore, the LA, TA, LO, and TO phonon nomenclature. Along with the basics behind the (quantum theory of) radiation–matter interaction and the concept of the bond polarizability (or ease of distorting the bonding electrons from their original positions), a full (group theory) description of these modes is outside the scope of this work and the interested reader is advised to look for further information in [8,12,14,16,82]. That being said, the above phenomenological description of the Raman scattering effect just paves the way to discuss the results that follow. Likewise, the discussion will be restricted to the main characteristics of the current semiconductor samples and experimental conditions – with the exception of the diamond-related results that have been retrieved from previous work [83] and from the literature [84] (see SuppInfo_Diamond).

Regardless of the size, type, or complexity all parts of Nature are made of atoms and, as expected, their main properties result from the number, characteristics and interaction of their constituent atoms. The distinctive optical bandgap of semiconductors, for example, originates from the covalent (sometimes, partially ionic) bonding between atoms, in which electrons can occupy either valence or conduction bands separated by an energy gap [85]. As a result, in pure semiconductors, a minimum energy (corresponding to the energy gap) is required so that the bonding electrons can be excited from the valence to the conduction band and contribute to the optical absorption process. This optical bandgap energy E_{gap} is proportional to the typical bonding energy E_{bond} between the constituent atoms and it presents different scaling rates depending whether the semiconductors are IV-IV-, III-V- or II-VI-based compounds [86] – see Fig. S19(a) in SuppInfo_Associations. Similar correspondences can be found in the literature connecting the E_{gap} (and, ultimately, E_{bond}) of some semiconductors with their infrared absorption and Raman frequencies [87–89], as well as with certain light emitting processes [90,91].

Applied to the present study, the Raman peak positions of the phonon modes considered so far (including the results of diamond) are represented in Fig. 5(a) as a function of E_{gap} – all of them at RT. According to the figure: higher $\omega(RT)$ values are consistent with increasing E_{gap} (or E_{bond} – see Fig. S19(b) in SuppInfo_Associations) and with some of the semiconductors main features – in a clear allusion to the quantum harmonic oscillator picture (*i.e.*, $\omega \propto \sqrt{E_{bond}}$ and $\omega \propto \sqrt{\mu^{-1}}$). An alternative way to observe the phonon–E_{gap} behavior is by representing the (linear, above RT) $d\omega/dT$ slope values *versus* E_{gap} (Fig. 5(b)) and respective dE_{gap}/dT slopes (Fig. 5(c)).

In this case: whereas there is no obvious (single) connection involving $d\omega/dT$ and E_{gap} (Fig. 5(b)), the $d\omega/dT$ *versus* dE_{gap}/dT results (Fig. 5(c)) suggest that, despite some data dispersion, the semiconductors presenting the lower T-dependent phonon variations are those in which the most significant T-dependent E_{gap} changes apply, and *vice-versa*. It happens owing to the specifics of each semiconductor but, most probably, because of the Bose-Einstein phonon population factor in determining the phonon–phonon (ω) and electron–phonon (E_{gap}) interactions. Another way to examine the data of Fig. 5(c) involves their relative variations *i.e.*, by considering "$d\omega/dT$ divided by $\omega(RT)$" *versus* "dE_{gap}/dT divided by $E_{gap}(RT)$" – as shown in Fig. S19(c) in SuppInfo_Associations. Now, at least for the IV-IV- and III-V-based compounds, the variations scale with each other and increase as the "reduced mass μ" of the semiconductors augment. A different behavior applies to the II-VI-based compounds, in which the relative "dE_{gap}/dT divided by $E_{gap}(RT)$" variation remains practically constant, while "$d\omega/dT$ divided by $\omega(RT)$" seems to increase with μ. Relating to the observed experimental data dispersion of Fig. 5 (and Fig. S19) it may arise due to the different phonon modes-symmetries (ω_{TO},ω_{LO}, etc.), to the various crystal structures (diamond, zinc blende, wurtzite, and rutile) and/or orientations, to the quasi-metallic character of some compounds (like InAs, for instance), or to a combination of these factors. In spite of that, it is notable to distinguish some connection between the ω- and E_{gap}-related experimental results.

In analogy with the preceding discussion, the Raman peak line-width $\gamma(RT)$ and $d\gamma/dT$ data were analyzed in terms of $E_{gap}(RT)$ and dE_{gap}/dT and they are shown in Fig. 6 (and Fig. S20 in SuppInfo_Associations).

This time, however, the dispersion of the experimental data prevents any reliable statement – except, maybe, some scaling-up of $d\gamma/dT$ in the IV-IV- and II-VI-based semiconductors at increasing dE_{gap}/dT variations (Fig. 6(c)). In this case, the absence of any evident relationship is not surprising and it simply emphasizes the effect of different phonon modes-symmetries and crystal structures-orientations in detriment of a plain γ-related behavior. Moreover, the influence of nearby phonon modes (particularly during the curve fitting of the Raman spectra) should not be ignored as a potential source of error in obtaining accurate γ values. Nevertheless, the above Raman and E_{gap} results (and related discussion) can be very useful in proposing two applications and operating ranges for the considered semiconductor materials.

The first of these applications involves the use of semiconductors to develop optical thermometers, the second one refers to the construction of interferometric (tunable) filters.

In principle, any material can function as a thermometer as long as some of its (physical, electrical, optical, magnetic, etc.) properties can be

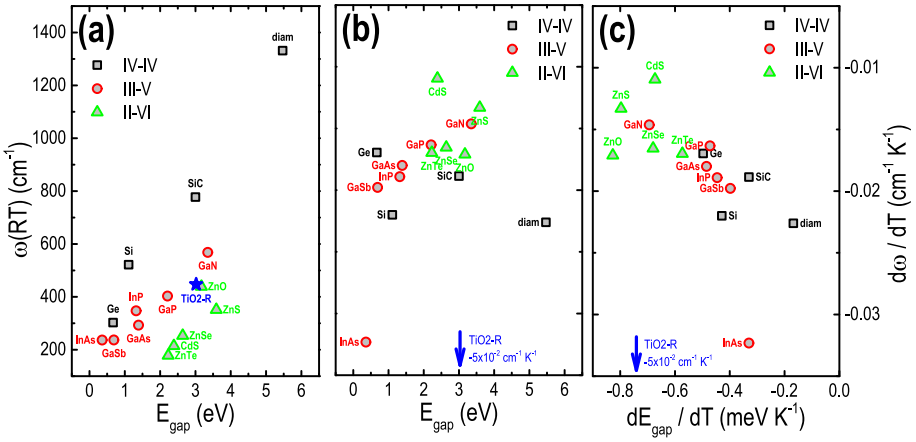

Fig. 5. (a) Room-temperature (RT) Raman peak position (or frequency ω) as a function of the optical bandgap E_{gap} of some IV-IV-, III-V- and II-VI-based semiconductors – together with TiO_2-R. Above RT, linear $d\omega/dT$ slope values of previous semiconductors as a function of their respective (b) optical bandgaps (at RT), and (c) linear (above RT) dE_{gap}/dT slopes.

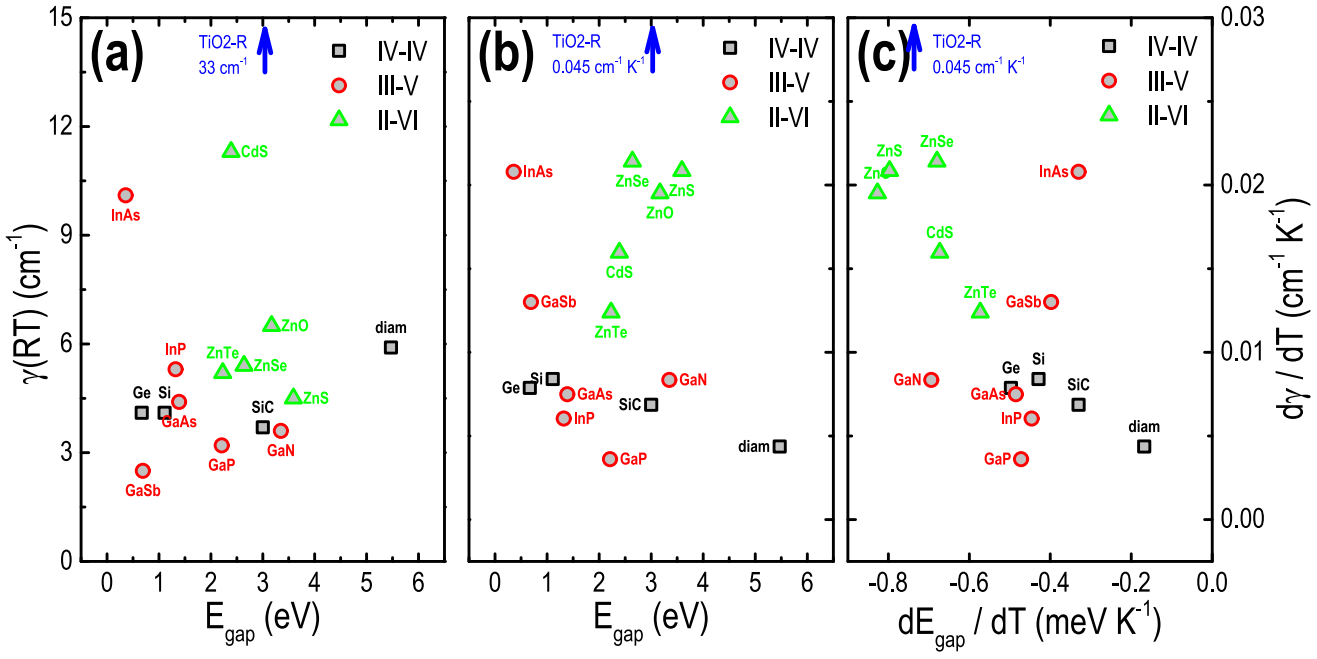

Fig. 6. (a) Room-temperature (RT) Raman peak line-width γ as a function of the optical bandgap E_{gap} of some IV-IV-, III-V- and II-VI-based semiconductors – together with TiO_2-R. Above RT, linear $d\gamma/dT$ slope values of previous semiconductors as a function of their respective (b) optical bandgaps (at RT), and (c) linear (above RT) dE_{gap}/dT slopes.

standardized in terms of a reference temperature source [92]. Within these, the optical properties are compatible with non-contact temperature measurements that, in addition, may offer speed, high sensitivity, reliability and linearity over a considerable range [93]. Depending on the instrumentation available, precision and T-range required various types of materials apply, so the temperature can be obtained by analyzing the spectral characteristics (signal wavelength-frequency-energy, intensity, shape, etc.) of certain optical processes [94] – such as those involving Raman scattering [95,96] or optical absorption [97,98], for example. Based on this, the semiconductor materials that present the highest (above-RT) $d\omega/dT$ and dE_{gap}/dT variations and, therefore, the most significant spectral changes in order to efficiently probe the temperature are (Fig. 5(c)): TiO_2-R (with$d\omega/dT = -0.04751$ cm^{-1} K^{-1}) and ZnO ($dE_{gap}/dT = -0.827$ meV K^{-1}). Other options include: InAs ($d\omega/dT = -0.03232$ cm^{-1} K^{-1}), diamond ($d\omega/dT = -0.02261$ cm^{-1} K^{-1}) and Si ($d\omega/dT = -0.02200$ cm^{-1} K^{-1}), as well as ZnS ($dE_{gap}/dT = -0.797$ meV K^{-1}) and TiO_2-R ($dE_{gap}/dT = -0.767$ meV K^{-1}) – see Table IV in SuppInfo_T-Variations.

Still relating to the optical properties of matter, tunable filters belong to a family of devices that, besides filtering, can control and modulate light and that can be used directly or integrated into a variety of photonic systems [99]. Basically, these filters consist of a series of thin films stacked together (also known as a distributed Bragg reflector DBR) so their individual refractive index (n), thickness (t), and final arrangement define a precise optical transmission or reflection range of wavelengths [100]. In the form of an optical resonator (*i.e.*, a layered structure in which a spacer is sandwiched between two DBR's), a well-defined optical transmission/reflection window develops around a preset photon wavelength λ_0 ($= 2n_{spacer}t_{spacer}$, for example [101]). Since n, E_{gap}, and t are temperature-sensitive, small variations of the external temperature induce changes in the optical window wavelength λ_0 and shape such that light filtering (and/or modulation) can be precisely adjusted-controlled. (Strictly, the temperature-dependent spectral characteristics of any interferometric – tunable filter rely on $n(T)$, or on the thermo-optic coefficient TOC – see [102] and Fig. S21 in SuppInfo_TOC.) Within this context, the semiconductors presenting the highest (above-RT) dn/dT values (corresponding to the $-0.020 < d\omega/dT < -0.015$ cm^{-1} K^{-1} range – see Fig. 5(b) in conjunction with Fig. S21 in SuppInfo_TOC) are supposed to provide tunable filters able to work over broader spectral ranges, as induced by the temperature. Within them, one can mention: Ge, Si, and most of the III-V-based compounds with $E_{gap} < 2.5$ eV. Coincidentally, these correspond to the semiconductors exhibiting the lowest $d\gamma/dT$ (<0.01 cm^{-1} K^{-1}) variations (Fig. 6(b)). If, instead, device operation requires high optical spectral stability against thermal variations, the wide bandgap materials (diamond, GaN, SiC, and most of the II-VI-based compounds) seem to be more appropriate. At this point it is important to notice that, unfortunately, the absence of TOC data of all the semiconductors considered in this work prevents a thorough analysis of the effect. Besides, these are just ideas to illustrate the potential of the information provided by Raman spectroscopy in planning a semiconductor-based device. In the specific case of an optical (thermometer or tunable filter) device, its definite composition – design has to take into account details like, for example: the working range – involving both temperature and spectral characteristics – precision and time-response required, as well as the instrumentation (and environmental conditions) available.

Concluding remarks

The Raman spectra of 15 semiconductor samples were measured, in the 83−823 K temperature range, by means of 632.8 nm laser excitation, backscattering geometry and no preferential polarization. The work considered IV-IV (Si, Ge, and SiC), III-V (GaN, GaP, GaAs, GaSb, InP, and InAs) and II-VI (ZnO, ZnS, ZnSe, ZnTe, and CdS) compounds, that included diamond, zinc blende, wurtzite and rutile (TiO_2) crystal structures. The temperature-dependent behavior of the most important phonon modes of the samples were analyzed in terms of their peak position (ω) and line-width (γ), as provided by fitting the experimental spectra with Voigt functions. In its current form this work presents, in a single document, all relevant Raman data (and references) of some of the most influential semiconductor materials in terms of basic and applied research. Moreover, according to the experimental data: (1) the $\omega(T)$ and $\gamma(T)$ results are consistent with the 3- and 4-phonon model (in the whole 83−823 K range) showing the influence of phonon–phonon and

thermal processes onto the phonon scattering behavior of the samples; (2) above room-temperature, the anharmonic phonon–phonon interaction prevails in most of the samples and provokes systematic changes in both $\omega(T)$ and $\gamma(T)$; (3) these changes are properly described by straight lines (namely, $d\omega/dT$ and $d\gamma/dT$ slopes) that present some correspondence with the optical bandgap E_{gap} of the semiconductors. Altogether, the experimental data are strictly related with the fundamental (chemical-physical) properties of the semiconductor samples and emphasize the effect of temperature onto the phonon–phonon (in determining both ω and γ) and electron–phonon (E_{gap}) processes. Additionally, they show the importance of Raman spectroscopy in providing important structural-electronic information that has been considered to (briefly) illustrate the suitability of certain semiconductors to applications involving the remote measurement of temperature (*i.e.*, by means of an optical thermometer) as well as in order to obtain temperature-(in) dependent optical filtering-modulation.

Author statements

Antonio Ricardo Zanatta has conceived, conducted the whole experimental work, and wrote/edited the manuscript.

CRediT authorship contribution statement

A.R. Zanatta: Writing – review & editing, Writing – original draft, Visualization, Validation, Resources, Project administration, Methodology, Investigation, Funding acquisition, Formal analysis, Data curation, Conceptualization.

Funding

This work was financially supported by the Brazilian agencies CNPq and FAPESP.

Declaration of competing interest

The authors declare that they have no known competing financial interests or personal relationships that could have appeared to influence the work reported in this paper.

Acknowledgments

This work was financially supported by the Brazilian agencies CNPq (Grant 304569/2021-6) and FAPESP.

Appendix A. Supplementary data

Supplementary data to this article can be found online at https://doi.org/10.1016/j.rinp.2025.108341.

Data availability

Data will be made available on request.

References

[1] Hoddeson L, Braun E, Teichman J, Weart S, editors. Out of the Crystal Maze: Chapters from the History of Solid-State Physics. NY: Oxford Univ. Press; 1992. ISBN 0-19-505329-X.
[2] Orton J. *The Story of Semiconductors*. Oxford: Oxford Univ. Press; 2009.
[3] Siffert P, Krimmel EF, Editors. In: Silicon: Evolution and Future of a Technology (Springer, Berlin, 2004). https://doi.org/10.1007/978-3-662-09897-4.
[4] Harrison WA. *Electronic Structure and the Properties of Solids – the Physics of the Chemical Bond* (Freeman. NY: W. H. & Comp; 1980.
[5] Sze SM, Ng KK. in Physics of Semiconductor Devices. NY: John-Wiley & Sons; 2006.
[6] Ashcroft NW, Mermin ND. *Solid State Physics*. FL: Harcourt College Publishers; 1976.
[7] Kittel C. *Introduction to Solid State Physics*. NY: John-Wiley & Sons Inc.; 2005.
[8] Yu PY, Cardona M. In: Fundamentals of Semiconductors: Physics and Materials Properties, Springer, Berlin, Heidelberg; 2010. https://doi.org/10.1007/978-3-642-00710-1.
[9] Grundmann M. in: The Physics of Semiconductors: An Introduction Including Nanophysics and Applications, Springer, Berlin, Heidelberg; 2010. https://doi.org/10.1007/978-3-642-13884-3.
[10] Böer KW, Pohl UW. Semiconductor Physics (Springer Cham) 2020. https://doi.org/10.1007/978-3-319-06540-3.
[11] Singh J. in *Physics of Semiconductors and their Heterostructures*. Singapore: McGraw-Hill Inc.; 1993.
[12] Parker SP, editor. *Spectroscopy Source Book*. NY: McGraw-Hill Inc.; 1988.
[13] Smith AL. in *Applied Infrared Spectroscopy: Fundamentals, Techniques, and Analytical Problem solving*. NY: John-Wiley & Sons; 1976.
[14] Laserna JJ, editor. *Modern Techniques in Raman Spectroscopy*. Chichester: John-Wiley & Sons; 1996.
[15] Long DA. Intensities in Raman spectra I. A bond polarizability theory. Proc Royal Soc A 1953;217:203–21. https://doi.org/10.1098/rspa.1953.0057.
[16] Szymanski HA, editor. Raman Spectroscopy: Theory and Practice. NY: Plenum Press; 1967.
[17] Madelung O, Schulz M, Weiss H, editors. In *Physics of Group IV Elements and III-V Compounds*: Semiconductors, Landolt–börnstein, New Series III/17a. Berlin, Heidelberg: Springer; 1982.
[18] Martienssen W, Warlimont H, Editors. In: Springer Handbook of Condensed Matter and Materials Data: Springer Handbooks (Springer, Berlin, Heidelberg 2005). https://doi.org/10.1007/3-540-30437-1_9.
[19] Madelung O, Schulz M, Weiss H, editors. In *Physics of II-VI and I-VII Compounds, Semimagnetic Semiconductors*: Semiconductors, Landolt–börnstein, New Series III/17b. Berlin, Heidelberg: Springer; 1982.
[20] Adachi S. in *Handbook on Physical Properties of Semiconductors - II-VI Compounds*. NY: Kluwer Academic Pub; 2004.
[21] Madelung O, Schulz M, Weiss H, editors. Semiconductors, Physics of Non-Tetrahedrally Bonded Binary Compounds III, Landolt–börnstein, New Series III/17g. New York, Tokyo: Springer, Berlin, Heidelberg; 1982.
[22] Pankove JI. in *Optical processes in semiconductors*. New York: Dover Pub; 1971.
[23] Zanatta AR. Revisiting the optical bandgap of semiconductors and the proposal of a unified methodology to its determination. 11225–12 pp Sci Rep 2019;9. https://doi.org/10.1038/s41598-019-47670-y.
[24] Goetzberger A, Knobloch J, Voβ B. in *Crystalline silicon solar cells*. Chichester: John Wiley & Sons; 1998.
[25] Zanatta AR. The Shockley–Queisser limit and the conversion efficiency of silicon-based solar cells. 100320–7 pp Res Opt 2022;9. https://doi.org/10.1016/j.rio.2022.100320.
[26] Siew SY, Li B, Gao F, Zheng HY, Zhang W, Guo P, et al. Review of silicon photonics technology and platform development. J. Lightwave Technol. 2021;39:4374–89. https://doi.org/10.1109/JLT.2021.3066203.
[27] Zalba MFG, Franceschi S, Charbon E, Meunier T, Vinet M, Dzurak AS. Scaling silicon-based quantum computing using CMOS technology. Nat. Electron. 2021;4:872–84. https://doi.org/10.1038/s41928-021-00681-y.
[28] Burkard G, Ladd TD, Pan A, Nichol JM, Petta JR. Semiconductor spin qubits. 025003–58 pp Rev. Mod. Phys. 2023;95. https://doi.org/10.1103/RevModPhys.95.025003.
[29] Zhang JJ, Ni J. Germanium. Ref Mod Mater Sci Mater Eng 2016:1–11. https://doi.org/10.1016/B978-0-12-803581-8.02433-4.
[30] Scappucci G, Kloeffel C, Zwanenburg FA, Loss D, Myronov M, Zhang JJ, et al. The germanium quantum information route. Nat Rev Mater 2021;6:926–43. https://doi.org/10.1038/s41578-020-00262-z.
[31] Kimoto T, Cooper JA. in *Fundamentals of Silicon Carbide Technology: growth, Characterization, and applications*. John Wiley & Sons; 2014.
[32] She X, Huang AQ, Lucia O, Ozpineci B. Review of silicon carbide power devices and their applications. IEEE Trans Industrial Electron 2017;64:8193–205. https://doi.org/10.1109/TIE.2017.2652401.
[33] L. S. Pan and D. R. Kania (Eds), in Diamond: Electronic Properties and Applications (Springer, NY, 1995). https://doi.org/10.1007/978-1-4615-2257-7.
[34] Schwander M, Partes K. A review of diamond synthesis by CVD processes. Diam & Rel Mater 2011;20:1287–301. https://doi.org/10.1016/j.diamond.2011.08.005.
[35] Kalish R. Diamond as a unique high-tech electronic material: difficulties and prospects. J. Phys. D Appl. Phys. 2007;40:6467–78. https://doi.org/10.1088/0022-3727/40/20/S22.
[36] Mohammad SN, Salvador AA, Morkoc H. Emerging gallium nitride based devices. Proceed IEEE 1995;83:1306–55. https://doi.org/10.1109/5.469300.
[37] Roccaforte F, Leszczynski M. In: Introduction to Gallium Nitride Properties and Applications, in *Nitride Semiconductor Technology: Power Electronics and Optoelectronic Devices*. Berlin: Wiley VCH Verlag; 2020. https://doi.org/10.1002/9783527825264.ch1.
[38] Hart PB. In: Gallium Phosphide, in *Electronics Design Materials*. London: Palgrave Macmillan; 1971. https://doi.org/10.1007/978-1-349-01176-6_16.
[39] Wang Y, Pan Z, Yan Y, Yang Y, Zhao W, Ding N, et al. A review of gallium phosphide nanophotonics towards omnipotent nonlinear devices. Nanophotonics 2024;13:3207–52. https://doi.org/10.1515/nanoph-2024-0172.
[40] Blakemore JS. Semiconducting and other major properties of gallium arsenide. J Appl Phys 1982;53:R123–81. https://doi.org/10.1063/1.331665.
[41] Brozel M. Gallium arsenide. In: Kasap S, Capper P, editors. *Springer Handbook of Electronic and Photonic Materials*. Boston: Springer; 2006. https://doi.org/10.1007/978-0-387-29185-7_23.

[42] Laudise RA. Crystal growth progress in response to the needs for optical communications. J Crystal Growth 1983;65:3–23. https://doi.org/10.1016/0022-0248(83)90031-3.

[43] Dutta PS, Bhat HL, Kumar V. The physics and technology of gallium antimonide: an emerging optoelectronic material. J Appl Phys 1997;81:5821–70. https://doi.org/10.1063/1.365356.

[44] Milnes AG, Polyakov AY. Review - Gallium antimonide device related properties. Sol St Electron 1993;36:803–18. https://doi.org/10.1016/0038-1101(93)90002-8.

[45] Spitzer MB, Dingle B, Dingle J, Morrison R. A review of indium phosphide space solar cell fabrication technology. IEEE Conf Photovoltaic Specialists 1990;1:196–206. https://doi.org/10.1109/PVSC.1990.111617.

[46] Navazi ZR, Omidi Y, E M, Davaran S. Cadmium-free quantum dot-based theranostics. TrAC Trends Anal Chem 2019;118:386–400. https://doi.org/10.1016/j.trac.2019.05.041.

[47] Wang S, Li Y, Chen J, Lin O, Niu W, Yang C, et al. Development and challenges of indium phosphide-based quantum-dot light-emitting diodes. 100588–21 pp J Photochem Photobiol C: Photochem Rev 2023;55. https://doi.org/10.1016/j.jphotochemrev.2023.100588.

[48] M. P. Mikhailova, Indium arsenide (Chapter 7), in Handbook Series on Semiconductor Parameters, M. Levinshtein, S. Rumyantsev, and M. Shur (Eds). (World Scientific, 1996). https://doi.org/10.1142/9789812832078_0007.

[49] Jalali HB, DeTrizio L, Manna L, DiStasio F. Indium arsenide quantum dots: an alternative to lead-based infrared emitting nanomaterials. Chem Soc Rev 2022;51:9861–81. https://doi.org/10.1039/d2cs00490a.

[50] Ozgur U, Alivov YI, Liu C, Teke A, Reshchikov MA, Dogan S, et al. A comprehensive review of ZnO materials and devices. 041301–103 pp J Appl Phys 2005;98. https://doi.org/10.1063/1.1992666.

[51] F. Rahman, Zinc oxide light-emitting diodes: A review. Opt Eng 58 (2019) 1, 010901-20pp. https://doi.org/10.1117/1.OE.58.1.010901.

[52] Malik MA. Compound semiconductors: Chalcogenides. Comprehensive Inorganic Chemistry II: from Elements to Applications - 2013;4:177–210. https://doi.org/10.1016/B978-0-08-097774-4.00411-3.

[53] Sadovnikov SI. Synthesis, properties and applications of semiconductor nanostructured zinc sulfide. Russ Chem Rev 2019;88:571–93. https://doi.org/10.1070/RCR4867.

[54] Sun C, Gu Y, Wen W. and Lijuan Zhao, ZnSe based semiconductor core-shell structures: from preparation to application. Opt Mater 2018;81:12–22. https://doi.org/10.1016/j.optmat.2018.05.005.

[55] Cao YL, Liu ZT, Chen LM, Tang YB, Luo LB, Jie JS, et al. Single-crystalline ZnTe nanowires for application as high-performance green/ultraviolet photodetector. Opt Express 2011;19:6100–8. https://doi.org/10.1364/OE.19.006100.

[56] S. P. Mondal and S. K. Ray, in *Cadmium Sulfide Nanostructures for Device Applications* (Lambert Academic Publishing, 2010). ISBN-10 3843359490.

[57] Nowotny J. in *Oxide Semiconductors for Solar Energy Conversion - Titanium Dioxide*. FL: CRC Press; 2012.

[58] Kang X, Liu S, Dai Z, He Y, Song X, Tan Z. Titanium dioxide: from engineering to applications. 191–32 pp Catalysts 2019;9. https://doi.org/10.3390/catal9020191.

[59] Menendez J, Cardona M. Temperature dependence of the first-order Raman scattering by phonons in Si, Ge, and α-Sn: Anharmonic effects. Phys Rev B 1984;29:2051–9. https://doi.org/10.1103/PhysRevB.29.2051.

[60] A. Debernardi, C. Ulrich, M. Cardona, and K. Syassen, Pressure dependence of Raman linewidth in semiconductors, Phys Stat Sol (B), 223 (2001) 213-223. https://doi.org/10.1002/1521-3951(200101)223:1<213::AIDPSSB213>3.0.CO;2-I.

[61] R. L. McCreery, Dispersive Raman spectrometers, in Raman Spectroscopy for Chemical Analysis (Wiley-Interscience, NY, 2000). Chapter 4. ISBN 0-471-25287-5.

[62] Klein PB, Chang RK. Comparison of second-order Raman scattering measurements with a phonon density-of-states calculation in GaSb. Phys Rev B 1976;14:2498–502. https://doi.org/10.1103/PhysRevB.14.2498.

[63] Mooradian A, Wright GB. First order Raman effect in III–V compounds. Sol St Commun 1966;4:431–4. https://doi.org/10.1016/0038-1098(66)90321-8.

[64] Lemos V, Argüello CA, Leite RCC. Resonant Raman scattering of TO(A1), TO(E1) and E2 optical phonons in GaN. Sol St Commun 1972;11:1351–3. https://doi.org/10.1016/0038-1098(72)90541-8.

[65] Porto SPS, Fleury PA, Damen TC. Raman spectra of TiO_2, MgF_2, ZnF_2, FeF_2, and MnF_2. Phys Rev 1967;154:522–6. https://doi.org/10.1103/PhysRev.154.522 &.

[66] Lan T, Tang X, Fultz B. Phonon anharmonicity of rutile TiO_2 studied by Raman spectrometry and molecular dynamics simulations. 094305–11 pp Phys Rev B 2012;85. https://doi.org/10.1103/PhysRevB.85.094305.

[67] Taylor W. The Raman spectra of cubic zinc selenide and telluride. Phys. Lett. A 1967;24:556–8. https://doi.org/10.1016/0375-9601(67)90837-7.

[68] LaCombe JL, Irwin JC. The temperature dependence of the optical phonon linewidths and frequencies in ZnSe and ZnTe. Sol St Commun 1970;8:1427–31. https://doi.org/10.1016/0038-1098(70)90712-X.

[69] Irwin JC, LaCombe J. Phonon dispersion in ZnSe. Can J Phys 1972;50:2596–604. https://doi.org/10.1139/p72-34.

[70] Nilsen WG. Raman spectrum of cubic ZnS. Phys Rev 1969;182:838–50. https://doi.org/10.1103/PhysRev.182.838.

[71] Damen TC, Porto SPS, Tell B. Raman effect in zinc oxide. Phys Rev 1966;142:570–4. https://doi.org/10.1103/PhysRev.142.570.

[72] Arguello CA, Rousseau DL, Porto SPS. First-order Raman effect in wurtzite-type crystals. Phys Rev 1969;181:1351–63. https://doi.org/10.1103/PhysRev.181.1351.

[73] Calleja JM, Cardona M. Resonant Raman scattering in ZnO. Phys Rev B 1977;16:3753–61. https://doi.org/10.1103/PhysRevB.16.3753.

[74] Temple PA, Hathaway CE. Multiphonon Raman spectrum of silicon. Phys Rev B 1973;7:3685–97. https://doi.org/10.1103/PhysRevB.7.3685.

[75] Carles R, Saint-Cricq N, Renucci JB, Renucci MA, Zwick A. Second-order Raman scattering in InAs. Phys Rev B 1980;22:4804–15. https://doi.org/10.1103/PhysRevB.22.4804.

[76] Poulet H, Mathieu JP. Détermination des vibrations fondamentales du sulfure de cadmium cristallisé. Ann Phys 1964;13:549–52. https://doi.org/10.1051/anphys/196413090549.

[77] Cerdeira F, Cardona M. Effect of carrier concentration on the Raman frequencies of Si and Ge. Phys Rev B 1972;5:1440–54. https://doi.org/10.1103/PhysRevB.5.1440.

[78] S. Nakashima and H. Harima, Raman investigation of SiC polytypes. phys stat sol (a) 162 (1997) 39-64. https://doi.org/10.1002/1521-396X(199707)162:1<39::AID-PSSA39>3.0.CO;2-L.

[79] See, for example Zanatta AR. Raman spectroscopy of lithium niobate ($LiNbO_3$) – sample temperature and laser spot size effects. Res Phys 2023;47:106380–8. https://doi.org/10.1016/j.rinp.2023.106380.

[80] Klemens PG. Anharmonic decay of optical phonons. Phys Rev 1966;148:845–8. https://doi.org/10.1103/PhysRev.148.845.

[81] At this point it is worth noticing that: (1) strictly, the lattice expansion effects (as proposed by the 3- and 4-phonon model) only applies for cubic systems, in which the thermal expansion coefficient is isotropic, and (2) both the magnitude and signal of the Ω's and Γ's constants (again, as proposed by the 3- and 4-phonon model) can be related with the softening-hardening of the phonon modes, as well as with their effective coupling. None of these aspects have been considered and, together with the experimental-modeling limitations just mentioned, the results relating the model are merely illustrative.

[82] Smith E, Dent G. in *Modern Raman Spectroscopy - a Practical Approach*. UK: John-Wiley & Sons; 2005.

[83] Joya MR, Zanatta AR, Ortega JB. Raman spectroscopy of temperature-induced effects in four carbon allotropes. 1350203–10 pp Mod Phys Lett B 2013;27. https://doi.org/10.1142/S0217984913502035.

[84] Cheng L, Zhu S, Ouyang X, Zhengh W. Bandgap evolution of diamond. 109638–5 pp Diam Rel Mater 2023;132. https://doi.org/10.1016/j.diamond.2022.109638.

[85] Cox PA. *The Electronic Structure and Chemistry of Solids*. NY: Oxford Univ Press; 1987.

[86] Manca P. A relation between the binding energy and the band-gap energy in semiconductors of diamond or zinc-blende structure. J Phys Chem Sol 1961;20:268–73. https://doi.org/10.1016/0022-3697(61)90013-0.

[87] Zanatta AR, Chambouleyron I. Nitrogen in the amorphous-germanium network: from high dilution to the alloy phase. Phys Rev B 1993;48:4560–70. https://doi.org/10.1103/PhysRevB.48.4560.

[88] Zanatta AR, Chambouleyron I, Santos PV. Study of structural changes in amorphous germanium–nitrogen alloys by optical techniques. J Appl Phys 1996;79:433–8. https://doi.org/10.1063/1.360849.

[89] Chambouleyron I, Zanatta AR. Nitrogen in germanium. J Appl Phys 1998;84:1–30. https://doi.org/10.1063/1.368612.

[90] Zanatta AR. Photoluminescence quenching in Er-doped compounds. Appl Phys Lett 2003;82:1395–7. https://doi.org/10.1063/1.1557318.

[91] Zanatta AR. A sensitive temperature probe based on Er^{3+}-doped GeO_x films. 102871–4 pp Res Phys 2020;16. https://doi.org/10.1016/j.rinp.2019.102871.

[92] Schooley JF. in *Thermometry*. Boca Raton USA: CRC Press Inc.; 1988.

[93] Zanatta AR, Scoca D, Alvarez F. A suitable (wide-range + linear) temperature sensor based on Tm^{3+} ions. 14113–8 pp Sci Rep 2017;7. https://doi.org/10.1038/s41598-017-14535-1.

[94] Brites CDS, Lima PP, Silva NJO, Millan A, Amaral VS, Palacio F, et al. Thermometry at the nanoscale. 4799–31 pp Nanoscale 2012;4. https://doi.org/10.1039/c2nr30663h.

[95] Y. Ozawa, S. Yamamoto, T. Fukahori, H. Kumugiyama, K. Sugiyama, T. Tsutsui, K. Hashiba, S. Endoh, H. Kawakami, A. Tokushima, and K. Yamazaki, Fiber optic distributed temperature sensor system. US Patent 5.113.277 (May 12, 1992).

[96] Zanatta AR. Temperature-dependent Raman scattering of the Ge+GeO_x system and its potential as an optical thermometer. 103500–9 pp Res Phys 2020;19. https://doi.org/10.1016/j.rinp.2020.103500.

[97] R. A. Frosh and M. M. Sharma, Optical crystal temperature gauge with fiber optic connections. US Patent 4.338.516 (July 6, 1982).

[98] Zanatta AR. The optical bandgap of lithium niobate ($LiNbO_3$) and its dependence with temperature. 105736–3 pp Res Phys 2022;39. https://doi.org/10.1016/j.rinp.2022.105736.

[99] Domash L, Wu M, Nemchuk N, Ma E. Tunable and switchable multiple-cavity thin film filters. J. Lightwave Technol. 2004;22:126–35. https://doi.org/10.1109/JLT.2004.823349.

[100] MacLeod MA. Thin-Film Optical Filters. Bristol: Institute of Physics; 2001.

[101] Gallo IB, Zanatta AR. A simple-versatile approach to achieve all-Si-based optical micro-cavities. 083106–7 pp J Appl Phys 2013;113. https://doi.org/10.1063/1.4793592.

[102] Zanatta AR, Gallo IB. The thermo optic coefficient of amorphous SiN films in the NIR and VIS regions and its experimental determination. 042402–4 pp Appl Phys Exp 2013;6. https://doi.org/10.7567/APEX.6.042402.